

Supplemental Material

Article: Reservoir-Induced Seismicity in China: Systematic Characterization and Implications for Hazard Assessment

Authors: Jiashan Zhang, Changsheng Jiang*, Fengling Yin, Yiming Zhu, Hongyu Zhai, Jinmeng Bi, Yan Zhang

*Corresponding Author: Changsheng Jiang (jiangcs@cea-igp.ac.cn)

S1. Data compilation and spatial representativeness of the screening sample

The China Reservoir Dataset (CRD) contains 97,435 vectorized reservoirs nationwide (Song *et al.*, 2022). The present study focuses on the 4,854 medium and large reservoirs with a Reservoir Capacity of at least $0.1 \times 10^8 \text{ m}^3$. Critical engineering parameters—including initial impoundment date, dam height, and reservoir capacity—were compiled by integrating multi-source heterogeneous data (*e.g.*, academic literature, the Encyclopedia of Chinese Rivers and Lakes, local gazetteers, government reports, and news archives) and subjected to rigorous cross-validation.

Of these 4,854 reservoirs, 1,435 possess complete records for the required parameters and initial impoundment dates falling between 1 January 1971 and 27 March 2015, thereby satisfying the dual requirements of at least one year of pre-impoundment and ten years of post-impoundment seismic data. The remaining 3,419 reservoirs were excluded, either because essential parameters were missing or because their impoundment dates lay outside the study window. Among the excluded reservoirs with incomplete parameter records, 1,997 were identified; notably, 1,433 of these (71.76%) have a capacity below $0.3 \times 10^8 \text{ m}^3$. Data coverage is nearly comprehensive for large reservoirs (capacity $\geq 1 \times 10^8 \text{ m}^3$): 746 such reservoirs are included in the final sample, representing 84.29% of all large reservoirs in the CRD. At the medium-reservoir level, 2,111 entries were compiled, accounting for 53.39% of the corresponding CRD population.

Figure S1 compares the spatial distributions of the full 4,854-reservoir set, the 1,435-reservoir screening sample, and the 3,419 excluded reservoirs. The three maps exhibit closely similar geographic patterns, with the highest reservoir densities concentrated in southwestern China (notably the Sichuan–Yunnan region and the eastern Tibetan Plateau margin), along the middle and lower Yangtze River corridor, and in southeastern coastal provinces. Because the excluded reservoirs are not preferentially clustered in any tectonically distinct region relative to the full set, their omission does not introduce spatial bias into the national-scale characterization of induced-type reservoirs presented in the main text.

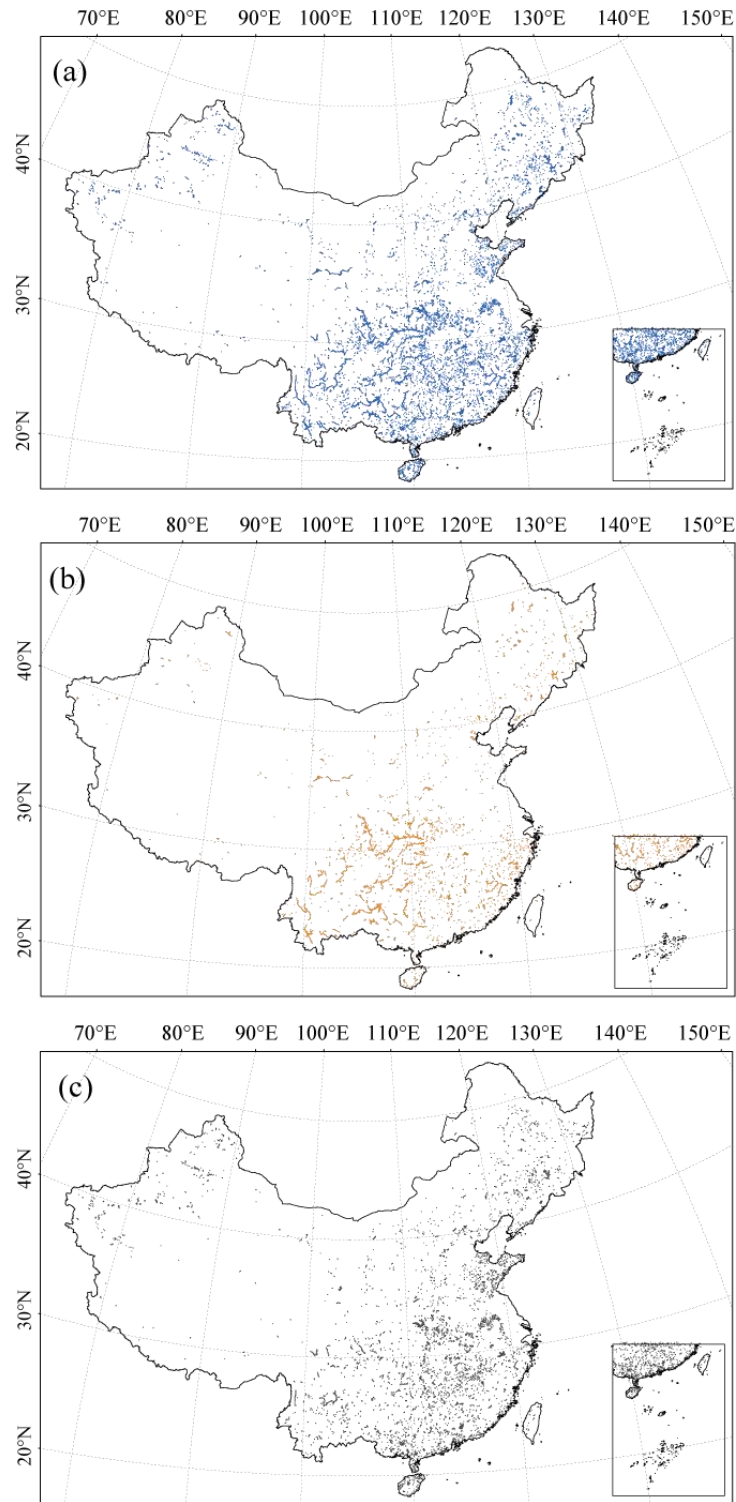


Fig. S1. Spatial representativeness of the reservoir screening sample. (a) Spatial distribution of all 4,854 medium and large reservoirs (Reservoir Capacity $\geq 0.1 \times 10^8 \text{ m}^3$) in the CRD. (b) Spatial distribution of the 1,435 retained reservoirs with complete parameters and initial impoundment dates between 1 January 1971 and 27 March 2015. (c) Spatial distribution of the 3,419 excluded reservoirs lacking complete information or falling outside the required impoundment time window. The similar geographic clustering across all three panels indicates that data exclusion does not preferentially remove reservoirs from any specific tectonic province, ensuring that the spatial patterns of induced-type reservoirs reported in the main text are not biased by the screening process.

S2. Validation of induced-seismicity identification and the W-score model across diverse reservoir settings

The main text establishes a unified identification framework that couples manual spatiotemporal clustering criteria with a probabilistic W-score model to systematically detect reservoir-induced seismicity (RIS) at the national scale. Operationally, three concurrent criteria are employed: (1) a significant post-impoundment increase in seismic frequency and intensity that is clearly distinguishable from pre-impoundment background levels; (2) pronounced spatial clustering of earthquakes, often exhibiting linear geometric features consistent with fault activation; and (3) close spatial association with the reservoir, typically within several tens of kilometers of the shoreline. While the Jinping-I Reservoir is presented in the main text as a representative illustration of this procedure, relying on a single case study inevitably limits the ability to assess the portability and robustness of the method across China's highly heterogeneous geological and hydrological environments. Indeed, the 88 identified induced-type reservoirs are distributed across markedly different tectonic regimes—from the high-strain eastern margin of the Tibetan Plateau to relatively stable intraplate blocks—and encompass a wide spectrum of reservoir geometries, ranging from narrow canyon-type impoundments to wide-valley configurations, and of storage capacities spanning more than an order of magnitude.

The **Xiluodu Reservoir**, a large (Type-1) canyon-type facility on the lower Jinsha River (capacity $126.7 \times 10^8 \text{ m}^3$, first impounded 4 May 2013), exhibits a pronounced post-impoundment cluster in its northeastern sector (purple dashed line, Fig. S2) where pre-impoundment seismicity was weak and small events subsequently showed spatiotemporal aggregation near the shoreline, whereas clusters in the northern ($\sim 20 \text{ km}$) and southwestern ($\sim 10 \text{ km}$) fault-proximal zones were excluded because strong background activity and proximity to active faults preclude unambiguous separation from natural tectonic earthquakes, a distinction corroborated by normalized frequency and cumulative-frequency analyses for $M_C = 2.0, 2.5,$ and 3.0 (Fig. S2b–c) and by the W-score table (Fig. S3), where induced earthquakes (circles) plot in the high-probability yellow-green region ($0.6 < W < 1.0$) and background events (squares) concentrate in the low-probability blue-cyan region ($W < 0.4$). The **Xiangjiaba Reservoir**, a large sinuous facility on the Jinsha River (capacity $51.63 \times 10^8 \text{ m}^3$, normal pool level $\sim 380 \text{ m}$, impounded 10 October 2012), similarly shows intensified post-impoundment microseismicity within its purple dashed boundary; although the central cluster lies near a seismogenic belt, its near-reservoir location and brief temporal separation from background activity support its classification as an induced sequence (minor background contamination may be present but does not affect the statistical results), with cumulative frequency curves

diverging ~250 days after impoundment (Fig. S4c), and its W-score distribution (Fig. S5) reproduces the high-versus-low segregation observed at Xiluodu. The **Guangzhao Reservoir** on the Beipan River in Guizhou Province (capacity 32.45×10^8 m³, compact geometry, no active faults within the image area, impounded December 2007) displays a marked post-impoundment cluster within ~10 km of the shoreline in a previously quiescent zone, a dominant distance peak at 0–4 km (Fig. S6b), and a delayed onset relative to background seismicity (Fig. S6c), with its W-score diagram (Fig. S7) again placing induced events in the high-W zone and background events in the low-W zone. Finally, the **Shuikou Reservoir** on the Min River in Fujian Province (capacity 23.4×10^8 m³, wide-valley type, no surface active faults, impounded 31 March 1993) generated dense swarms of micro-earthquakes within 10 km where background activity had been extremely weak (Fig. S8), a temporal delay verified by cumulative curves (Fig. S8c), and its W-score assessment (Fig. S9) shows the same induced-high/background-low pattern.

Collectively, these four supplementary cases demonstrate that the diagnostic signatures of reservoir-induced seismicity remain robust across markedly different geological settings, reservoir morphologies, and storage capacities. Despite variations in local tectonics—from active fault-intersected canyon reaches to stable blocks devoid of surface faulting—all four reservoirs exhibit induced sequences that display a sharp post-impoundment increase in activity, pronounced spatial clustering in near-shoreline zones, and temporal behavior clearly separable from background seismicity. Crucially, the W-score distributions consistently segregate these manually identified induced earthquakes into the high-W interval ($0.6 < W < 1.0$) while background natural tectonic earthquakes remain confined to the low-W region ($W < 0.4$). This congruence confirms that the manual selection boundaries are not arbitrary geometric delineations but reflect genuine seismogenic responses to reservoir impoundment that are independently recoverable by a quantitative probabilistic metric. Moreover, the spatial confinement of induced sequences to the near field and their characteristic temporal delay relative to impoundment further corroborate the pore-pressure-diffusion-dominated mechanism discussed in the main text, supporting the argument that the effective physical influence range of reservoir water extends considerably beyond the 10 km threshold currently prescribed in Chinese standards. By validating both the manual identification protocol and the W-score model under contrasting conditions, this supplementary section affirms that the combined methodology provides a reliable, reproducible framework for probabilistic RIS identification across China's diverse reservoir environments.

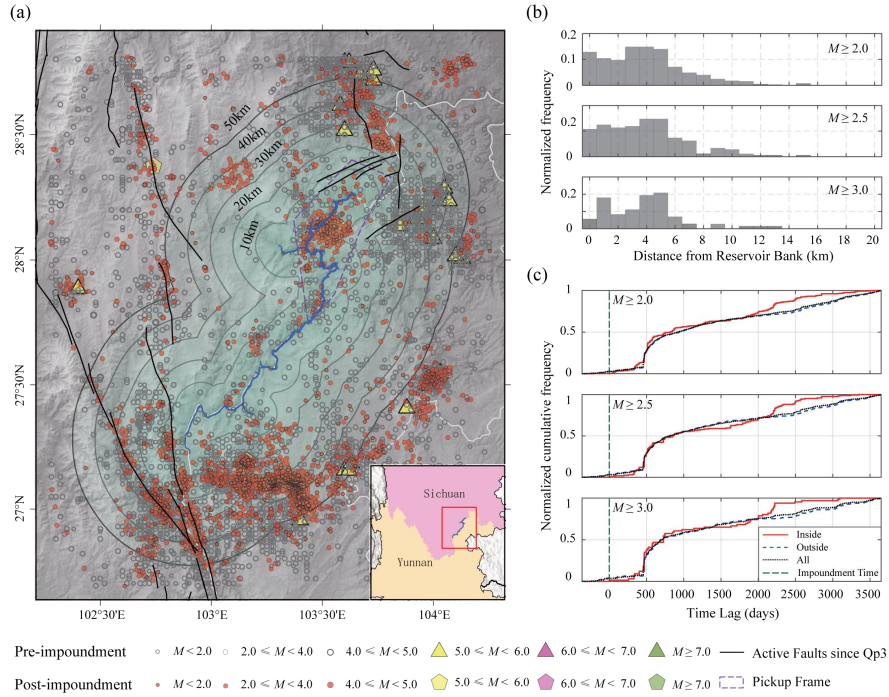


Fig. S2. Xiluodu Reservoir: example of induced seismicity sequence identification. (a) Reservoir boundary and spatial distribution of seismicity. Gray dots represent background seismicity recorded from 1970 to the initial impoundment (4 May 2013); red dots represent post-impoundment earthquakes; purple dashed lines outline the spatiotemporal cluster boundary of the induced sequence; black curves denote active faults since the Late Pleistocene; gradient green shading indicates zones within 10, 20, 30, 40, and 50 km of the reservoir shoreline. The inset shows the location of the study area. (b) Normalized frequency distribution of induced earthquakes as a function of distance from the reservoir shoreline (0~20 km range, 1 km bins). Subplots from top to bottom correspond to completeness magnitudes $M_C = 2.0, 2.5,$ and 3.0 . (c) Temporal comparison of cumulative earthquake frequency from one year before to ten years after initial impoundment. “Inside” denotes the induced sequence, “outside” denotes background seismicity, and “all” denotes all earthquakes; curves are normalized to their maximum values. The green vertical dashed line marks the time of initial impoundment. Subplots from top to bottom correspond to $M_C = 2.0, 2.5,$ and 3.0 .

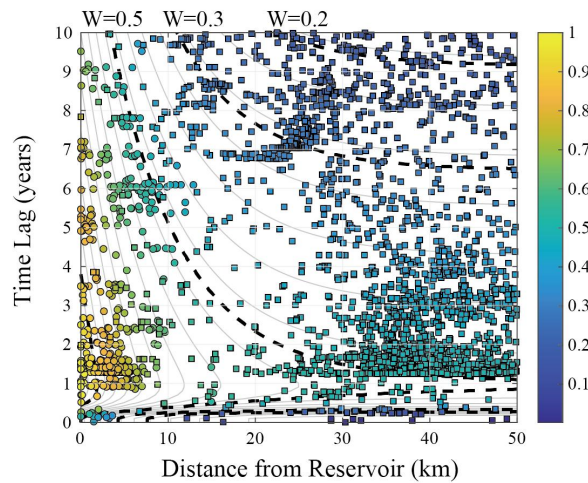


Fig. S3. Xiluodu Reservoir: W-score distribution of the earthquake catalog. Circles represent identified induced earthquakes, which cluster in the high-W yellow-green region; squares represent background earthquakes, concentrated in the low-W blue-cyan region.

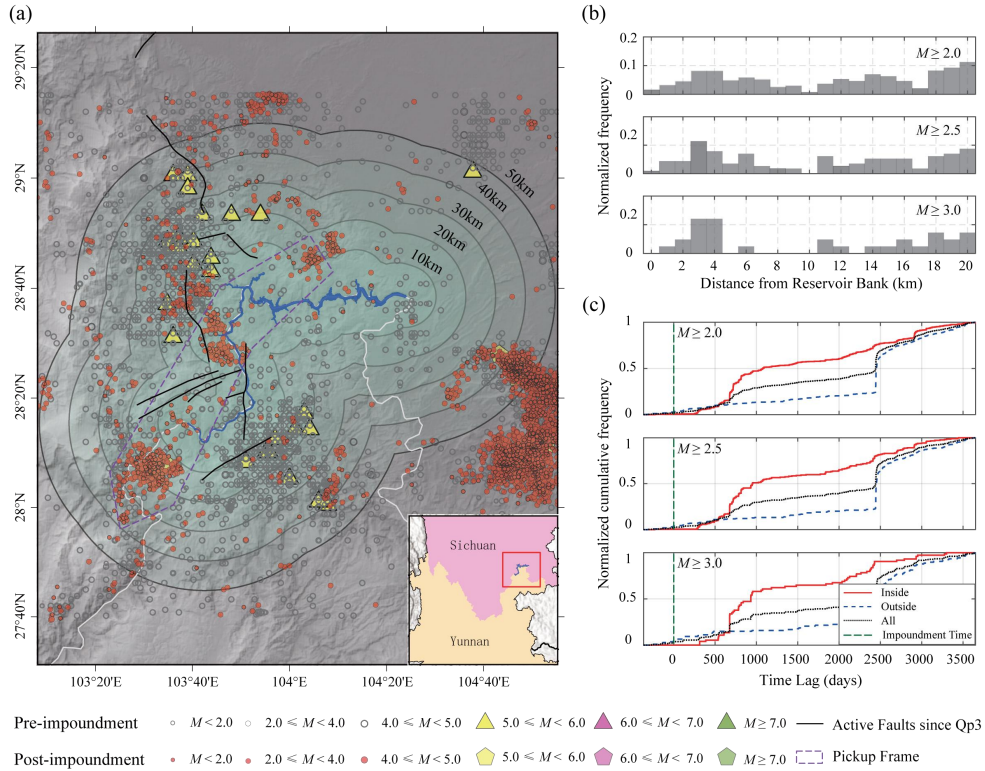


Fig. S4. Xiangjiaba Reservoir: example of induced seismicity sequence identification. Panel elements are identical to those in Fig. S2.

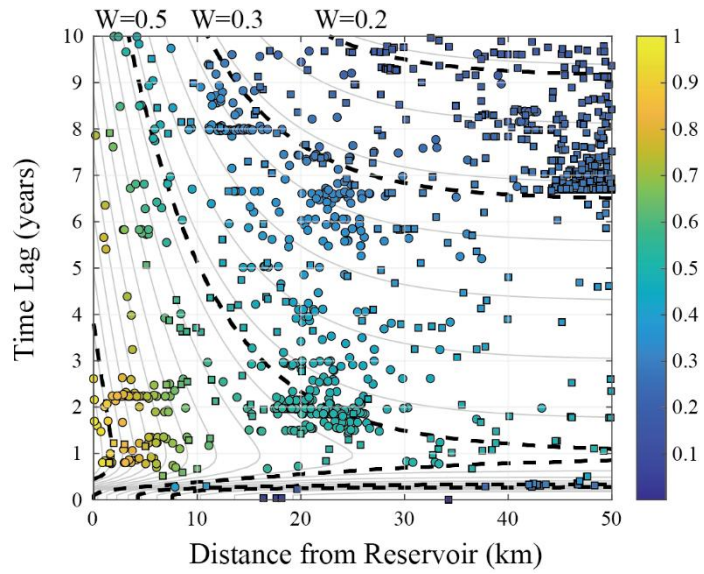


Fig. S5. Xiangjiaba Reservoir: W-score distribution. Symbols are as defined in Fig. S3.

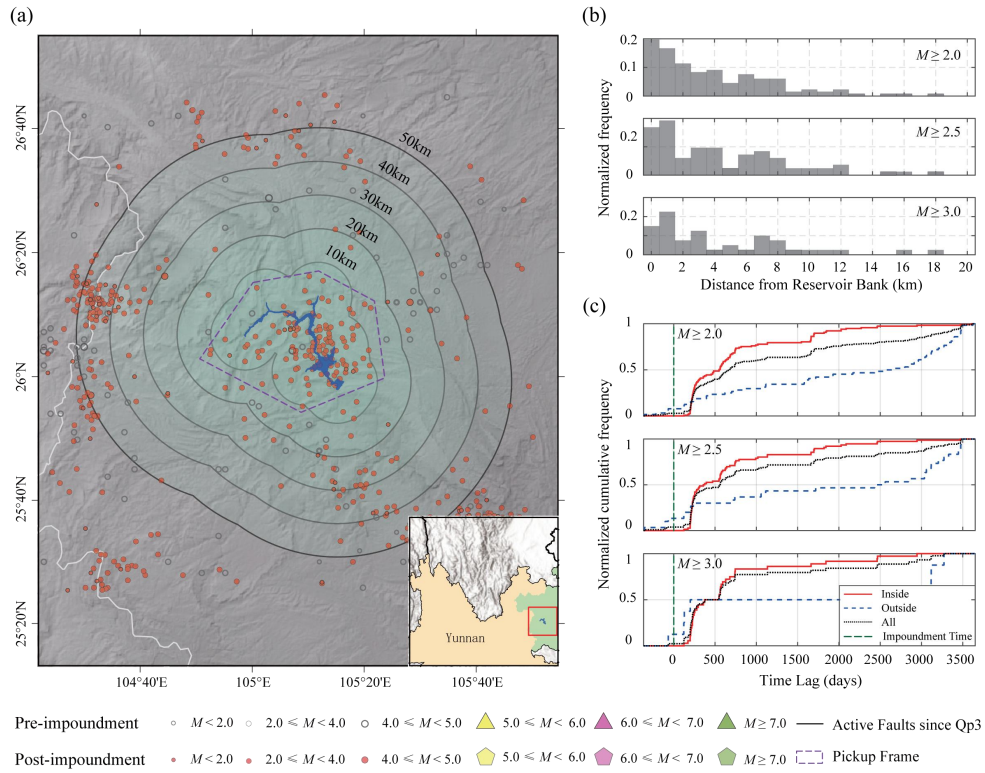


Fig. S6. Guangzhao Reservoir: example of induced seismicity sequence identification. Panel elements are identical to those in Fig. S2.

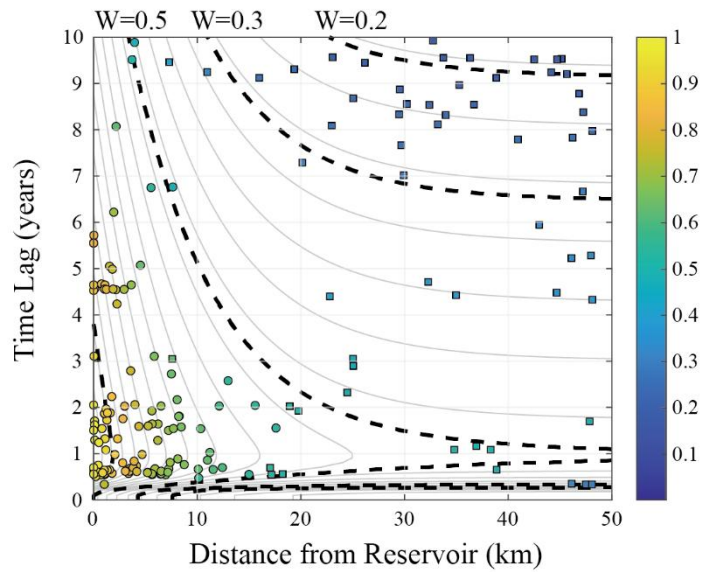


Fig. S7. Guangzhao Reservoir: W-score distribution. Symbols are as defined in Fig. S3.

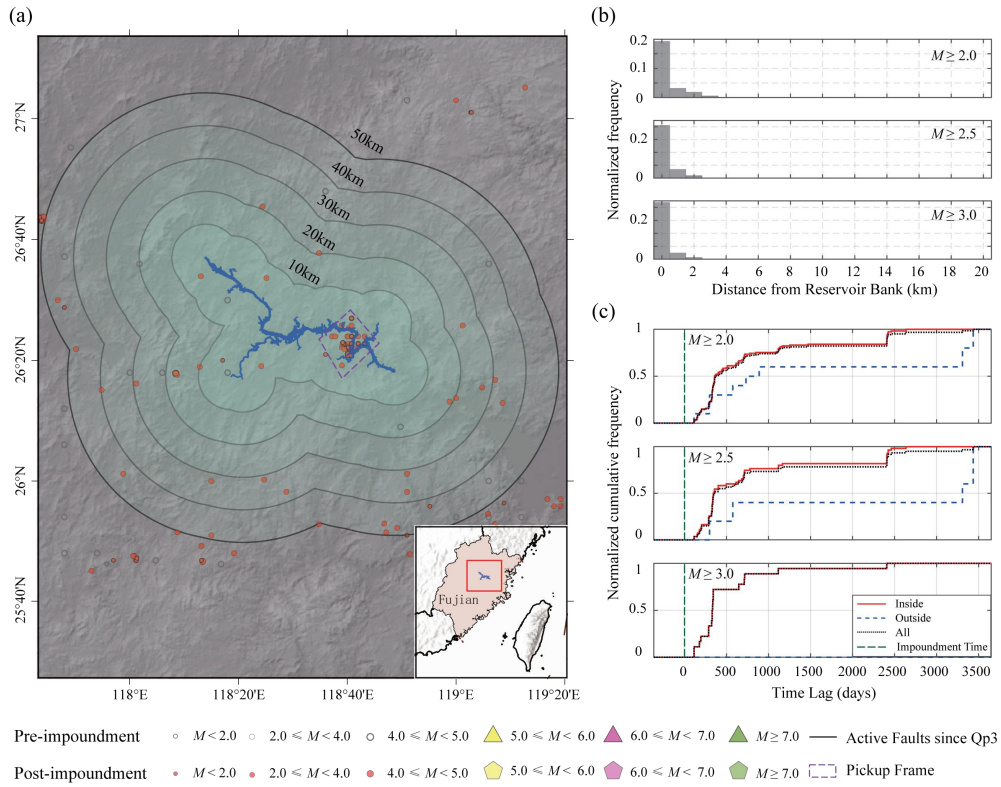


Fig. S8. Shuikou Reservoir: example of induced seismicity sequence identification. Panel elements are identical to those in Fig. S2.

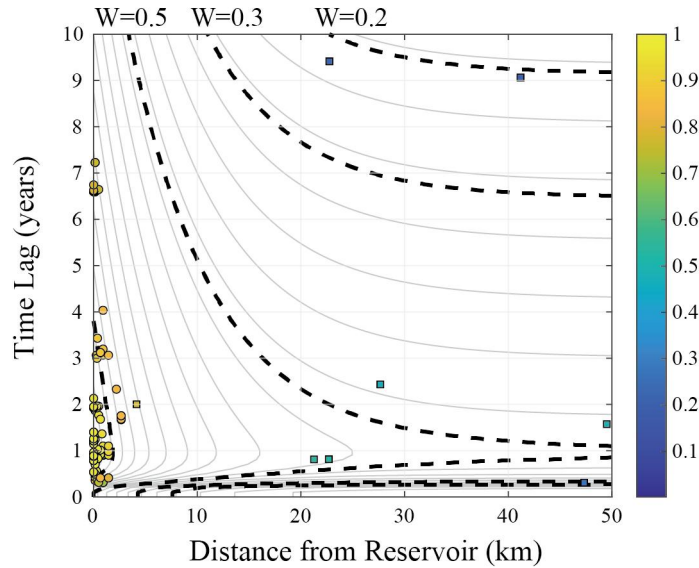


Fig. S9. Shuikou Reservoir: W-score distribution. Symbols are as defined in Fig. S3.

References

Song, C., Fan, C., Zhu, J., Wang, J., Sheng, Y., Liu, K., Chen, T., Zhan, P., Luo, S., Yuan, C., and Ke, L.: A comprehensive geospatial database of nearly 100 000 reservoirs in China, *Earth Syst. Sci. Data*, 14, 4017–4034, <https://doi.org/10.5194/essd-14-4017-2022>, 2022.